A&A 428, 579–586 (2004)
DOI: 10.1051/0004-6361:20041406

Astronomy & Astrophysics

A low upper-limit on the lithium isotope ratio in HD140283⋆

W. Aoki[1], S. Inoue[2,6], S. Kawanomoto[1], S. G. Ryan[3], I. M. Smith[3], T. K. Suzuki[1,4,7], and M. Takada-Hidai[5]

[1] National Astronomical Observatory, 2-21-1 Osawa, Mitaka, Tokyo 181-8588, Japan
e-mail: aoki.wako@nao.ac.jp;kawanomo@optik.mtk.nao.ac.jp;stakeru@scphys.kyoto-u.ac.jp
[2] Max-Planck-Institut für Astrophysik, Karl-Schwarzschild-Str. 1, 85741 Garching, Germany
e-mail: inoue@mpi-mpi-hd.mpg.de
[3] Centre for Earth, Planetary, Space and Astronomical Research, Dept of Physics & Astronomy, The Open University, Walton Hall, Milton Keynes, MK7 6AA, UK
e-mail: s.g.ryan@open.ac.uk
[4] Department of Astronomy, School of Science, University of Tokyo, 7-3-1 Hongo, Bunkyo-ku, Tokyo 113-0033, Japan
[5] Liberal Arts Education Center, Tokai University, 1117 Kitakaname, Hiratsuka-shi, Kanagawa, 259-1292, Japan
e-mail: hidai@apus.rh.u-tokai.ac,jp
[6] *Present adress:* Max-Planck-Institut für Kernphysik, Postfach 103980, 69029 Heidelberg, Germany
[7] *Present adress:* Department of Physics, Kyoto University, Kitashirakawa, Kyoto 606-8502, Japan

Received 20 January 2003 / Accepted 28 August 2004

Abstract. We have obtained a high-S/N (900–1100), high-resolving-power (R = 95 000) spectrum of the metal-poor subgiant HD 140283 in an effort to measure its ^{6}Li/^{7}Li isotope ratio. From a 1-D atmospheric analysis, we find a value consistent with zero, ^{6}Li/^{7}Li = 0.001, with an upper limit of ^{6}Li/^{7}Li < 0.018. This measurement supersedes an earlier detection (0.040 ± 0.015(1σ)) by one of the authors. HD 140283 provides no support for the suggestion that Population II stars may preserve their ^{6}Li on the portion of the subgiant branch where ^{7}Li is preserved. However, this star does not defeat the suggestion either; being at the cool end of the subgiant branch of the Spite plateau, it may be sufficiently cool that ^{6}Li depletion has already set in, or the star may be sufficiently metal poor that little Galactic production of ^{6}Li had occurred. Continued investigation of other subgiants is necessary to test the idea. We also consider the implications of the HD 140283 upper limit in conjunction with other measurements for models of ^{6}Li production by cosmic rays from supernovae and structure formation shocks.

Key words. stars: abundances – stars: Population II – Galaxy: halo – Galaxy: kinematics and dynamics – Galaxy: structure – nuclear reactions, nucleosynthesis, abundances

1. Introduction

Although the Big Bang is believed to be the major producer of the ^{7}Li seen in Population II (Pop. II) stars, it is not believed to be a significant source of the lighter isotope, ^{6}Li. A range of possible sites exist for ^{6}Li including not only spallative and fusion sources normally associated with supernova-accelerated Galactic cosmic rays (Walker et al. 1985; Steigman & Walker 1992), but also stellar flares (Deliyannis & Malaney 1995) and possibly shocks produced by large-scale-structure formation (Suzuki & Inoue 2002). Measurements of the ^{6}Li/^{7}Li ratio in metal-poor stars could therefore provide important constraints on Li production following the Big Bang. The isotope ratio can also constrain possible destruction of Li, since ^{6}Li is destroyed in stars at a lower temperature than ^{7}Li. ^{6}Li is more susceptible to destruction than ^{7}Li in some Li-depleting mechanisms (Deliyannis 1990), but not necessarily in slow-mixing models where the less-fragile elements ^{7}Li and ^{9}Be are depleted in concert with one another (Deliyannis et al. 1998). Consequently, reliable measurements of the Galactic evolution of ^{6}Li as well as ^{7}Li could have wide implications. Since the fusion mechanism (Steigman & Walker 1992) produces ^{6}Li without co-producing beryllium or boron, observations of Be (Boesgaard et al. 1999) and B (Duncan et al. 1997) do not adequately constrain Li production, especially at the earlier epochs where fusion was more important than spallation. Models of spallative production of Be and B are also affected by long-running uncertainties in the Galactic chemical evolution of the most relevant heavy nucleus, oxygen. Consequently, the yield of ^{6}Li/^{9}Be depends not only on the cosmic ray energy spectrum (which may include a substantial low energy component (LEC); Vangioni-Flam et al. 1994), confinement (Prantzos et al. 1993; Fields et al. 1994), the evolution with metallicity of the flux (Yoshii et al. 1997) and composition (Fields et al. 1994; Ramaty et al. 1997; Vangioni-Flam et al. 1999), but also on the fast particle and interstellar medium abundances.

⋆ Based on data collected at the Subaru Telescope, which is operated by the National Astronomical Observatory of Japan.

Depending on the particle source abundance distribution, the production ratio of ^{6}Li/^{9}Be ranges over 3–100 (Ramaty et al. 1996). Consequently, it is necessary to constrain ^{6}Li evolution directly from measurements of the ^{6}Li/^{7}Li ratio.

Unfortunately, the measurement of ^{6}Li in stellar spectra is very difficult. The 6707 Å transition, the only Li feature strong enough to permit an attempt, is a fine-structure doublet, and the isotopic displacement of the ^{6}Li lines from the ^{7}Li lines is comparable to both the doublet separation and to the intrinsic line width. The latter is determined primarily by thermal Doppler broadening in the hot stellar atmosphere and by poorly characterised non-thermal (turbulent) motions. These factors, combined with the low fraction (<10%) of ^{6}Li, mean that high-resolution, high-signal-to-noise spectra are required. Even then, stellar models (Deliyannis 1990), supported by observational evidence (Smith et al. 1993), indicate that ^{6}Li is depleted below detection levels in all but the hottest main-sequence, Pop. II stars. Finding Pop. II stars hot enough to preserve ^{6}Li and bright enough to yield high S/N at high spectral resolution has been difficult. Progress was made with 3- to 4-m telescopes during the last decade: Smith et al. (1993, 1998) find ^{6}Li/Li = 0.06 ± 0.03 in HD 84937 and ^{6}Li/Li = 0.05 ± 0.03 in BD+26°3578; Hobbs & Thorburn (1994, 1997) measure ^{6}Li/^{7}Li = 0.08 ± 0.04 in HD 84937; and Cayrel et al. (1999) obtain ^{6}Li/^{7}Li = 0.052 ± 0.019 in HD 84937. The reality of the ^{6}Li detection in HD 84937 is supported by an analysis of its K I 7698 Å line (Smith et al. 2001). Also important are the numerous non-detections in other stars reported in those works. Isotope ratios have also been measured for a number of metal-poor disc stars (Nissen et al. 1999). The advent of 8-m telescopes should improve the situation.

Deliyannis (1990, his Fig. 7) noted that ^{6}Li survival might also be high in subgiants containing Spite-plateau Li abundances, at least down to ~5800 K, since these stars had high effective temperatures on the main sequence. Deliyannis & Ryan (2000) set out to test this directly, and on the basis of a spectrum analysis by S.G.R. claimed a detection of ^{6}Li/^{7}Li at 0.040 ± 0.014(1σ) in the subgiant HD 140283. We set out to verify this observation and analysis using the new High Dispersion Spectrograph (HDS) on the Subaru 8.2-m telescope (Noguchi et al. 2002). In the following sections of this paper, we present data with a S/N around 1000 per pixel, and report our finding of a very low upper limit, ^{6}Li/^{7}Li < 0.018, which supersedes S.G.R.'s earlier analysis.

2. Observation

During commissioning of HDS, we sought a very high-S/N observation of HD 140283 to verify the earlier ^{6}Li detection at the same time as proving the capabilities of the new spectrograph. The spectrum was obtained over two nights, 22 and 29 July 2001, from thirteen exposures totalling 82 min. This gave a S/N = 900–1100 per 0.018 Å pixel around 6707 Å at $R \equiv \lambda/\Delta\lambda$ = 95 000, using a slit width of 0.4 arcsec (0.2 mm). The seeing was typically 0.55–0.6 arcsec, so the slit was well illuminated. This allows us to estimate the instrumental profile from the comparison spectrum, which we do below. The spectrum was wavelength calibrated using a ThAr spectrum, and gave typical RMS errors of 0.0015 Å.

3. Spectral analysis

3.1. General approach

Our procedure was to compare the observed data with synthetic spectra computed using code originating with Cottrell & Norris (1978) and a 1D model atmosphere grid by R.A. Bell (1983, private communication). A model with $T_{\rm eff}$ = 5750 K, $\log g$ = 3.4, [Fe/H] = −2.5, and microturbulence ξ = 1.4 km s^{-1} was used, along with the Li line list of Smith et al. (1998). Spectra were synthesised for various values of ^{6}Li/^{7}Li and convolved with macroturbulent and instrumental profiles. In order to do this we first determined the instrumental profile and then found (model-dependent) constraints on macroturbulence using procedures described in Sects. 3.2 and 3.3.

To determine the best fit when comparing synthetic and observed spectra, a χ^2 test was employed, where

$$\chi^2 \equiv \Sigma \left[\frac{(O_i - S_i)^2}{\sigma_i^2} \right]$$

and O_i is the observed continuum-normalised flux, S_i is the synthesised flux, and σ_i is the standard deviation of the observed points defining the continuum. From this we calculated the reduced χ^2, χ^2_r, defined as

$$\chi^2_r \equiv \frac{\chi^2}{(\nu - 1)}$$

where ν is the number of degrees of freedom (e.g. Smith et al. 1998). The best fit from a set of synthesised spectra is the one that minimises χ^2_r.

Once the observed spectra were normalised using neighbouring continuum windows, four variables affect the comparison between spectra: the abundance $A(X)$ of element X, the wavelength shift $\Delta\lambda$, the macroturbulence Γ, and the ^{6}Li/^{7}Li ratio. To determine these, several iterations are needed as they are dependent on each other at some level.

The wavelength shift $\Delta\lambda$ that is allowed for each line may have any of several possible origins: an error in the applied Doppler correction for the star's motion; errors in the wavelength calibration of the ThAr frame (rms = 0.0015 Å); an error in the wavelength of the line listed in the spectrum-synthesis linelist, which will differ from line to line; and possible variations in the motions of different elements, ionisation states, and excitation states in a dynamic, 3D, real stellar atmosphere. We return to these shifts below, in Sect. 3.3.

3.2. Instrumental profile

The instrumental profile was calculated from a ThAr hollow-cathode-lamp spectrum over the interval 6660–6730 Å taken with the same instrumentation setup as the stellar exposures. Nineteen emission lines of various strengths were isolated and normalised to the same strength by scaling them to the height of a fitted Gaussian. (In doing this we are not claiming that the ThAr profiles are Gaussian, merely that a Gaussian provides a useful reference profile for normalising their heights.) On closer examination it was noted that six had weak lines in their wings, significant enough to impact weakly on our estimate of the instrumental profile, and so were rejected from the

analysis. The remaining 13 unblended lines were then overlaid and averaged to give the instrumental profile shown in Fig. 1a. (The instrumental profiles for several setups have been given in Noguchi et al. 2002, our result is similar.) It is comforting that the lines give essentially identical profiles despite their different intensities. From the fall-off of the flux away from the line core, we believe that the lines effectively end around ±0.3 Å, but we chose to truncate our calculations at 0.2 Å. We estimate that <0.5% of the flux lies beyond ±0.2 Å.

Although we use the numerical profile in our stellar analysis, it is instructive to investigate analytic approximations. Standard deviations were calculated over the intervals $\Delta\lambda$ = ±0.1 and ±0.2 Å, the former giving σ = 0.030 Å and a tolerable fit to the line core, and the latter giving σ = 0.037 Å (Fig. 1b). The larger standard deviation associated with the wider interval arises because 1.5% of the flux within $\Delta\lambda$ = ±0.2 falls between ±0.1 and ±0.2, outside the 3σ interval, whereas a true Gaussian would have less than 0.3% beyond 3σ. This inflates the standard deviation if the Gaussian fit is evaluated out to ±0.2 Å. This shows that the instrumental profile has broader wings than a Gaussian. The effect of (optionally) assuming a Gaussian instrumental profile is addressed in the stellar analysis below.

Figure 1b also shows the bisector of the average instrumental profile to illustrate its symmetry. Without magnification one would say it was perfectly symmetric. After magnification by a factor of ten, a small s-shape can be seen through the profile, but for our purposes the profile can be regarded as symmetric.

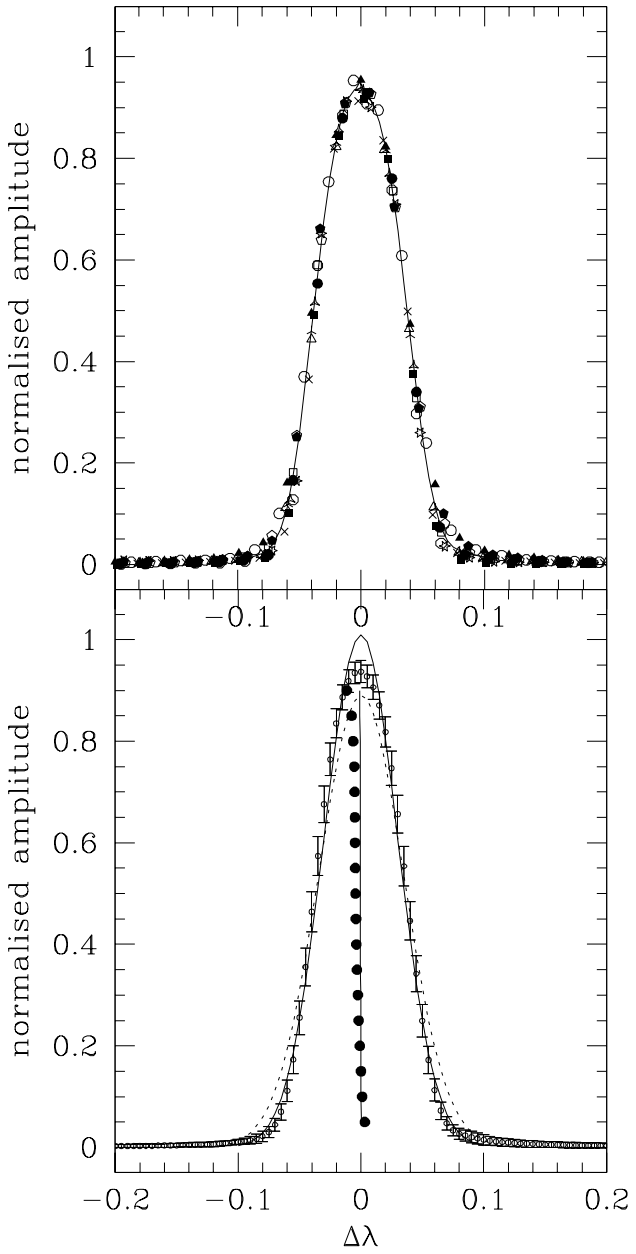

Fig. 1. a) *Points*: normalised flux versus distance from line centre for 13 ThAr lines. The peak intensity and central wavelength of each line was determined from a Gaussian fit. *Solid line*: numerical instrumental profile obtained as the unweighted average of the points. **b)** *Errorbars*: numerical instrumental profile and standard error of each value. *Solid curve*: Gaussian fit to instrumental profile over ±0.1 Å. *Dotted curve*: Gaussian fit to instrumental profile over ±0.2 Å. *Vertical line*: line bisector of the instrumental profile. *Filled dots*: line bisector enlarged ×10 in wavelength.

3.3. Macroturbulence

We sought to constrain the macroturbulence from stellar spectral lines other than Li, and convolved the synthetic spectrum with a Gaussian broadening function of FWHM Γ_1 km s^{-1} to model this. Synthetic spectra of five Ca I and Fe I lines (Table 1) were calculated iteratively to find values of A(Ca) (or A(Fe)), $\Delta\lambda$ and Γ_1 that minimised χ^2_r. As can be seen from Col. (6) of the table, the values of Γ_1 vary from line to line, but do not appear to correlate with atomic number, wavelength, excitation potential or equivalent width. It was noted that the Ca I 6717 Å line has a weak line in its long-wavelength wing that could not have been modelled simultaneously to the same precision, potentially degrading our results. Ca I 6717 also required a different $\Delta\lambda$ value, −8 mÅ compared to -18 ± 2 mÅ for the others[1]. It was therefore decided to average the other four lines to give the preferred macroturbulence, $\langle\Gamma_1\rangle$ = 4.65 km s^{-1}. The consistency of the $\Delta\lambda$ values for the four lines (excluding Ca I 6717) argues for a systematic error in the velocity correction applied during the data reduction as the source of the shift.

We also investigated the result of adopting a radial-tangential macroturbulent broadening profile, adopting the $\zeta_R = \zeta_T$ and $A_R = A_T$ prescription of Gray (1992, Chap. 18). The Ca I and Fe I lines examined above constrained ζ_{RT} to 4.21 ± 0.13 km s^{-1}, whereupon a value 4.20 km s^{-1} was adopted.

[1] Our analysis of the Ca I line assumed a wavelength of 6717.688 Å. Dr Bonifacio has kindly pointed out an unpublished measurement of the wavelength by Rosberg & Johansson, cited by Smith et al. (1998), giving the value 6717.677 Å, which is 11 mÅ less than we have used. Adopting the Rosberg & Johansson value would change the $\Delta\lambda$ value in Table 1 to −19 mÅ, which would be consistent with the other values. However, it would not alter the broadening values for the line, which also seem slightly anomalous, possibly due to the presence of a weak blend as noted in the text.

Table 1. Macroturbulence values for Ca and Fe lines.

Ion	λ	χ_{lo}	W	$\Delta\lambda$	Γ_1	Γ_c	Γ_2	ζ_{RT}
	Å	eV	mÅ	mÅ	km s^{-1}	km s^{-1}	km s^{-1}	km s^{-1}
(1)	(2)	(3)	(4)	(5)	(6)	(7)	(8)	(9)
Ca I	6162.18	1.9	37.6	−19	4.83	6.03	5.14	4.40
Ca I	6439.08	2.5	29.2	−19	4.60	5.75	5.10	4.10
Ca I	6717.69	2.7	4.2	−8	5.05	6.00	4.80	4.60
Fe I	6494.99	2.4	26.7	−18	4.60	5.73	4.78	4.20
Fe I	6678.00	2.7	12.4	−15	4.55	5.63	4.66	4.15
Average ± s.d. excl. 6717				−18 ± 2	4.65 ± 0.13	5.79 ± 0.17	4.92 ± 0.24	4.21 ± 0.13
Adopted					4.65	5.80		4.20

Notes:
Γ_1 = *FWHM* of Gaussian macroturbulence adopting numerical instrumental profile.
Γ_c = *FWHM* of composite Gaussian modelling macroturbulence and instrumental profile.
Γ_2 = *FWHM* of Gaussian macroturbulence assuming Γ_c incorporates a Gaussian instrumental profile with σ = 0.030 Å.

To test the sensitivity of the results to the commonly-used assumption of Gaussian profiles, the best fit for a single Gaussian broadening function to model both the instrumental profile and macroturbulence was also calculated. The FWHM of this composite Gaussian is denoted Γ_c. A similar spread in values for Γ_c as for Γ_1 was observed. These values gave $\langle\Gamma_c\rangle$ = 5.80 km s^{-1}. Since Γ_c represents a convolution of the instrumental profile with the supposed Gaussian macroturbulence Γ_2, Col. (8) in Table 1 estimates the macroturbulent portion assuming the instrumental profile is a Gaussian profile with a standard deviation of 0.03 Å (see Sect. 3.2).

3.4. Lithium isotope ratio

With the instrumental profile determined numerically and the macroturbulence Γ_1 constrained from four Ca and Fe lines, the synthesised and observed spectrum could be compared at Li 6707 Å. The χ^2 statistic was calculated over the 35 pixels from 6707.50 Å to 6708.20 Å, where the Li profile is distinguishable from the noise in the continuum. The continuum level was estimated out of this wavelength range. The effects of the uncertainties in the macroturbulence and the continuum level on the final results are estimated in Sect. 3.5.

The macroturbulence and the continuum level are two of the five free parameters determined by the profile fitting to the Li line in the analysis by Cayrel et al. (1999). However, the macroturbulence and the continuum level are, at least in principle, able to be determined independently of the Li line analysis. In contrast, the ^{6}Li and ^{7}Li abundances must be determined from the Li line analysis. Though the wavelength calibration and doppler correction can be made from the detailed analysis of spectral lines other than the Li line, there is still some uncertainty of the wavelengths of the line transitions. For this reason, the wavelength zero-point is also adjusted by the Li line analysis in the present work.

Calculations of χ^2_r were performed covering a reasonable range of isotope ratios, total Li abundances, and wavelength shifts. These reduce the number of degrees of freedom by three, to 32. It was found during early work using multiple sampling of the independent variable x, that plots of χ^2_r vs. x could be fit very well by a quadratic function, and hence the minimum value of χ^2_r and its corresponding x value could be found after a few calculations. This yielded ^{6}Li/^{7}Li = 0.001 as the best fit (see Table 2 and corresponding χ^2_r-plots in Fig. 2).

The procedure was repeated for the pure Gaussian instrumental profile, giving essentially the same result, ^{6}Li/^{7}Li = 0.002. It can be seen from Fig. 2 that adopting the pure Gaussian profile for the combined macroturbulent and instrumental profiles is in close agreement with the preferred result based on the numerical instrumental profile. The calculation using the numerical instrumental profile also gives a marginally smaller χ^2_r value.

To test whether the Ca and Fe lines gave a reasonable value of Γ_1 to use on the lithium lines, we performed a series of iterations on A(Li), $\Delta\lambda_{6707}$ and ^{6}Li/^{7}Li in which Γ_1 was also allowed to vary. The χ^2_r minimum was found for Γ_1 = 4.53 km s^{-1}, shown in Table 2. This lies within 1σ of the preferred value, 4.65 km s^{-1}. Allowing Γ_1 to vary used up another degree of freedom, but nevertheless put χ^2_r marginally below the value for when Γ_1 took the preferred value constrained by the Ca and Fe lines.

The lower broadening value weakens the wings of the profile and hence requires a higher ^{6}Li/^{7}Li ratio to fit the specific observation, but ^{6}Li/^{7}Li remained below 0.01. Even allowing $\Delta\lambda_{6707}$ and A(Li) to vary, we found an almost linear relation between the ^{6}Li/^{7}Li ratio inferred and the adopted Γ_1, ^{6}Li/^{7}Li = $-0.038\Gamma_1 + 0.1777$ over the interval $4.50 < \Gamma_1 < 4.80$; probably this relation holds over a much wider range of macroturbulent values.

Figure 3 compares the observational data to the best fitting model and related models having ^{6}Li/^{7}Li = 0.02 and 0.04.

We note that the equivalent width of the Li absorption line determined by the best-fit synthetic spectrum is 47.8 mÅ. This value agrees well with that derived by Ford et al. (2002) for the same spectrum (48.1 mÅ). We also note that, even though the Li abundances derived by the present analysis are given in

Table 2. Isotope ratios inferred from different spectral models.

Inst. profile (1)	Macroturb. constraint (2)	Macrot. km s^{-1} (3)	^{6}Li/^{7}Li (4)	χ^2_r (5)	A(Li) (6)	$\delta\lambda$ mÅ (7)
Preferred solution						
HDS	Ca & Fe	$\Gamma_1 = 4.65$	$0.001^{+0.025}_{-0.001}$	0.74	2.184	−28.4
Other explored solutions						
HDS	Li	$\Gamma_1 = 4.53$	0.005	0.71	2.181	−28.0
HDS	Ca & Fe	$\zeta_{RT} = 4.20$	−0.007	0.83	2.188	−29.2
Gauss.	Ca & Fe	$\Gamma_c = 5.80$	0.002	0.81	2.183	−28.3

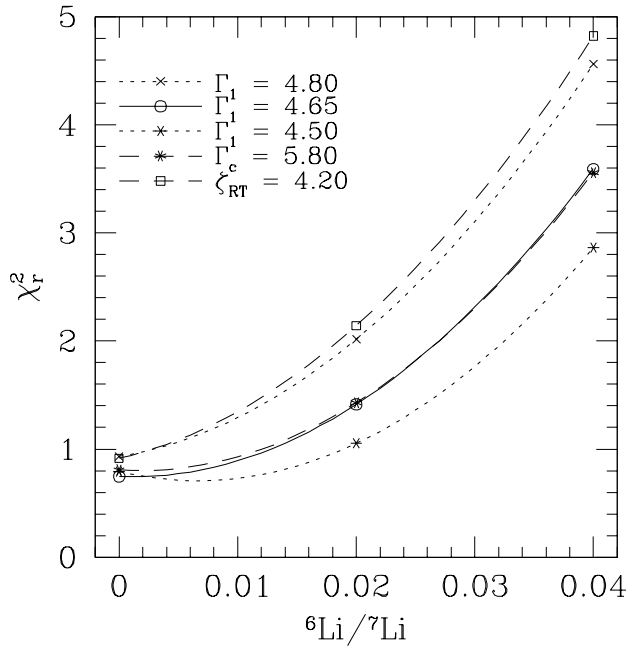

Fig. 2. χ^2_r values for five spectrum synthesis models as a function of input lithium isotope ratio. Points indicate the actual calculations, while curves give the fitted quadratic functions used to identify the minimum. *Solid curve*: preferred solution using numerical instrumental profile and Gaussian macroturbulence $\Gamma_1 = 4.65$ km s^{-1} constrained from four Ca and Fe lines. *Dotted curves*: solutions in which Γ_1 was varied to $\pm 1\sigma$ from the mean, to 4.50 and 4.80 km s^{-1}. *Dashed curves*: Alternative solutions in which (i) pure Gaussian functions were used for instrumental and macroturbulent broadening ($\Gamma_c = 5.80$ km s^{-1}); and (ii) the HDS instrumental profile and radial-tangential macroturbulence ($\zeta_{RT} = 4.20$ km s^{-1}) were assumed.

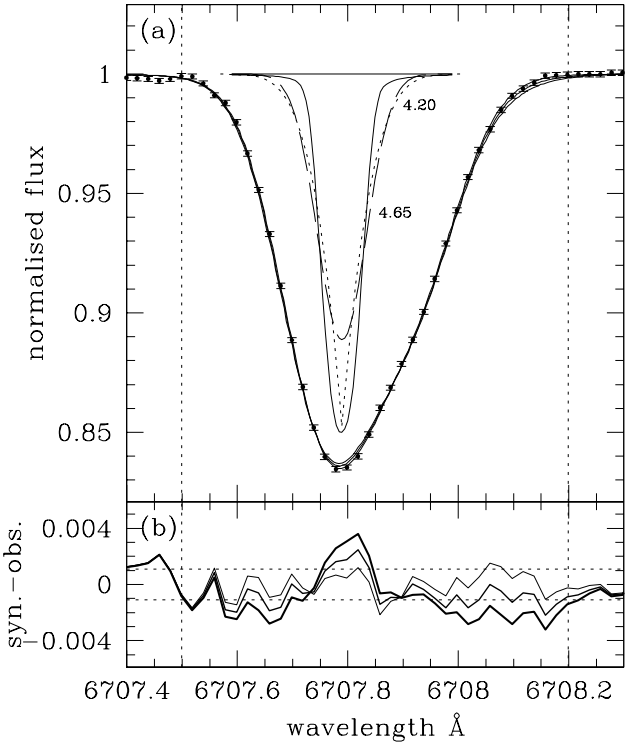

Fig. 3. a) Comparison of (*curves*) synthetic and (*filled circles*) observed Li-doublet spectra for the preferred, best-fitting model in Fig. 2 having ^{6}Li/^{7}Li = 0.00 and also models at 0.02 and 0.04. Note that the higher ^{6}Li/^{7}Li ratios demand lower ^{7}Li abundances, resulting in a weakening of the line core. The inset shows three equal-area broadening profiles for (*solid curve*) the HDS instrumental profile, (*dashed curve*) $\Gamma_1 = 4.65$ km s^{-1}, and (*dotted curve*) $\zeta_{RT} = 4.20$ km s^{-1}. The vertical dotted lines indicate the wavelength region over which the Li χ^2 analysis was conducted. **b)** Difference in normalised flux between synthetic and observed spectra. Light, medium and heavy lines correspond to ^{6}Li/^{7}Li = 0.00, 0.02 and 0.04 respectively. The horizontal dotted lines correspond to $\pm 1\sigma$ in the observed flux.

Table 2, the values are dependent on the choice of effective temperatures, while the isotope ratio is insensitive to the atmospheric parameters.

3.5. Uncertainties

We first estimate the statistical errors inherent in the spectrum with $S/N \simeq 1000$. We have tried to quantify this in two ways.

The first method is to consider the interpretation of the χ^2_r statistic. The probability that a χ^2 value as large as that measured should occur by chance is tabulated in many statistics books. Our plot of χ^2_r vs. ^{6}Li/^{7}Li for the preferred analysis method indicates that very low χ^2_r values were obtained at the best fitting isotope ratio, corresponding to high probabilities that random statistical fluctuations could produce χ^2 values this large. The random fluctuations modelled in the χ^2 formalism are, we recall, the σ values associated with the noise in

the continuum, in our case 0.0011. Away from the minimum, χ^2_r is larger and the probability that random fluctuations could produce such large χ^2 values decreases. For 32 degrees of freedom, the probability falls to 84.1% at $\chi^2_r = 1.325$, and to 97.8% at $\chi^2_r = 1.633$. These correspond to ^{6}Li/^{7}Li = 0.019 and 0.023, respectively, for the adopted value of $\Gamma = 4.65$ km s^{-1}.

However, due to the rebinning of the original spectra that occurs during data reduction, photon errors in adjacent pixels are not fully independent. As the χ^2 test assumes independent errors in adjacent pixels, the calculated chi-squared value is only an approximation to the value which ought to be minimised, as pointed out by Cayrel et al. (1999) and Bonifacio & Caffau (2003). We continue to use the χ^2 procedure and in particular select as our preferred parameter set that minimises the calculated χ^2_r value, but we are unable to associate a confidence interval to any particular chi-squared values that we calculate.

The second method involves conducting a Monte Carlo test in which a synthetic spectrum corresponding closely to the observed profile is subjected to Gaussian errors having the same distribution ($\sigma = 0.0011$) as the real data. A series of noisy, synthesised spectra based on a single input model are then subjected to the same χ^2-fitting procedures as the real analysis, to determine whether the input parameters can be recovered and with what accuracy. We performed 300 simulations to check the size of likely errors. Note that we are primarily interested in the spread of the results rather than the central value. For a synthetic spectrum having A(Li) = 2.223, a wavelength error $\Delta\lambda = 0.001$ Å, and ^{6}Li/^{7}Li = 0.014, we inferred the following parameters: A(Li) = 2.224 ± 0.001, $\Delta\lambda = 0.0012 \pm 0.0011$, and ^{6}Li/^{7}Li = 0.011 ± 0.004. The inferred isotope ratios deviate from the input value with an rms of 0.0042. This test suggests that, where the macroturbulence is constrained from other spectral features, the ^{6}Li/^{7}Li ratio can be recovered from data with $S/N = 900$ at an rms deviation = 0.0042. If the distribution of the results of the above simulation is assumed to be the Gaussian, the 3σ limit is 0.013 in the ^{6}Li/^{7}Li ratio.

The Monte Carlo estimate of the uncertainty in ^{6}Li/^{7}Li provides a smaller error than that inferred from the χ^2 statistic. Since the error estimate from the χ^2 approach contains a difficulty in our case as mentioned above, we adopt the value estimated by the Monte Carlo simulation (0.013 in the ^{6}Li/^{7}Li ratio) as the statistical error.

It is easy to calculate the effect of uncertain Γ values in the inferred ^{6}Li/^{7}Li ratio because, as noted above, there is a linear dependence of the isotope ratio on the assumed value. A characteristic uncertainty $\sigma_\Gamma = 0.15$ km s^{-1} translates to 0.006 in the isotope ratio.

We also estimated the errors due to the uncertainty of continuum normalization by changing the continuum level in the analysis. We found almost a linear correlation between the assumed continuum level and resulting ^{6}Li/^{7}Li ratio. The assumption of by 0.1% higher continuum results in by −0.010 lower ^{6}Li/^{7}Li ratio.

Combining the limit (^{6}Li/^{7}Li < 0.013) by the statistical error in quadrature with errors due to the uncertainties of macroturbulence and continuum level, we infer the upper limit of ^{6}Li/^{7}Li to be 0.018.

4. Discussion

The very low ^{6}Li/^{7}Li ratio found for HD 140283 is well below the value 0.040 ± 0.015 inferred by S.G.R. from an earlier analysis of poorer data (Deliyannis & Ryan 2000). S.G.R's previous analysis differed in several respects: the S/N was lower (435), and the sampling coarser (0.026 Å pix^{-1}), for the same resolving power. The reduction procedure also differed: in that work, an effort was made to constrain the fitting parameters independently rather than through a highly iterative χ^2 analysis as employed here. It is probable that the present procedure has resulted in better optimisation of the fitting parameters than was achieved in the previous work. Application of the current technique to the older spectrum gave ^{6}Li/^{7}Li = 0.011 when $\Gamma_c = 5.90$ km s^{-1} was constrained by the Ca I 6162 Å line, and 0.034 when $\Gamma_c = 5.38$ km s^{-1} was constrained by the Li I 6707 Å fit. These large variations in the inferred isotope ratio emphasise the need for good constraints on the macroturbulence if a reliable isotope fraction is to be obtained.

The analysis presented above is based solely on 1D model atmospheres. Analyses using 3D model atmospheres, which have begun to appear in recent years (e.g. Asplund et al. 1999), offer the hope of replacing the empirical micro- and macroturbulent parameters with physically-based velocity structures. The importance of this is clear from the strong correlation between the input (adopted) macroturbulent broadening and the output isotope ratio. It can only be hoped that 3D calculations will soon become commonly accessible to all stellar spectroscopists.

Deliyannis' suggestion that sufficiently warm subgiants might preserve their main-sequence ^{6}Li complement finds no support from the current observation, but nor is the suggestion necessarily defeated. At $T_{\rm eff} = 5750$ K, HD 140283 is very close to the effective temperature at which even ^{7}Li is seen to be diluted in subgiants (Pilachowski et al. 1993), so it is possible that ^{6}Li has begun to be depleted in this object. It is also amongst the most metal-poor of the stars in which ^{6}Li has been sought, so Galactic production may have been lower at this epoch. (Bear in mind, nevertheless, that ^{6}Li production via cosmic ray fusion is not as metallicity-dependent as production via spallation.) For these reasons it is still appropriate to examine warmer and/or higher-metallicity subgiants in an effort to detect ^{6}Li in them.

However, it is also possible that our upper limit reflects a genuinely low ^{6}Li abundance at production. On the premise that depletion has not been significant, and that the HD 140283 result is representative of stars in its metallicity range, we consider below the implications for different production models of Pop. II ^{6}Li. Figure 4 shows our data together with previously published results of ^{6}Li detections in HD 84937, BD+26°3578 and G271-162 (Smith et al. 1998; Nissen et al. 2000, and references therein). Also plotted are tentative detections for three additional stars from Asplund et al. (2001), CD–30°18140, G13-9 and HD160617, achieved through preliminary analysis of recent VLT/UVES observations. Note that although HD 140283 was additionally reported in Asplund et al. (2001) as a possible detection, their latest analysis for this star is

consistent with our limit here. Taken at face value, comparison of our upper limit with the other detections may suggest a relatively steep increase of ^{6}Li/H with metallicity near [Fe/H] $\simeq$ −2.4, followed by a slower rise. Alternatively, the data set may indicate typical ^{6}Li abundances that are a factor of 2–3 lower than the highest measured values, which may be consistent with previous upper limits for a few other stars (Smith et al. 1998; Hobbs et al. 1999).

The most widely discussed models so far for Pop. II ^{6}Li synthesis are based on spallation and/or fusion reactions induced by cosmic rays originating from supernovae (SNe). While they can successfully explain the Be and B observed in Pop. II stars, accounting for the observed ^{6}Li is rather problematic; they require either an implausibly high cosmic ray injection efficiency (Ramaty et al. 2000; Suzuki & Yoshii 2001), or the presence of an additional low energy cosmic ray component lacking observational support (Vangioni-Flam et al. 1999). Even if the typical values of ^{6}Li abundances turn out to be lower than the highest measurements by a factor of 2–3, the data would still significantly exceed conservative predictions of such models assuming standard SN CR energetics and spectra, drawn as a dashed line (D) in Fig. 4 (see Suzuki & Inoue 2002). In some secondary SN CR models, a steeply rising log(^{6}Li/H) − [Fe/H] relation can occur depending on the uncertain O-Fe relation (Fields & Olive 1999), but this is highly unlikely at the observed abundance levels in this metallicity range.

A very different scenario for ^{6}Li production has recently been put forth by Suzuki & Inoue (2002): nuclear reactions induced by cosmic rays accelerated at structure formation (SF) shocks, i.e. gravitational virialization shocks driven by the infall and merging of gas in sub-Galactic haloes during hierarchical build-up of structure in the early Galaxy. Such shocks are inevitable consequences of the currently standard theory of structure formation in the universe. Estimates for the specific energy dissipated at the main SF shock accompanying the final major merger give $\epsilon_{\rm SF} \simeq 0.4$ keV per particle, compared to that for early SNe at $\epsilon_{\rm SN} \sim 0.15$ keV per particle. Thus SF shocks can be potentially more energetic than SNe at early Galactic epochs, and the associated CRs can explain the ^{6}Li observations more naturally. Since such shocks do not eject freshly synthesized CNO nor Fe, $\alpha - \alpha$ fusion is the dominant production channel at low metallicities, which can generate large amounts of ^{6}Li with little Be or B and no direct correlation with Fe. A unique evolutionary behavior can arise, whereby ^{6}Li increases quickly at low metallicity (reflecting the main epoch of Galactic SF), followed by a plateau or a slow rise, in marked contrast to SN CR models for which log (^{6}Li/H) vs. [Fe/H] can never be much flatter than linear. Shown in Fig. 4 are three possible model curves for different parameter values of $t_{\rm SF}$, the main epoch of Galactic SF relative to halo chemical evolution, $\tau_{\rm SF}$, the main duration of SF, and $\gamma_{\rm SF}$, the spectral index of injected particles (see Suzuki & Inoue 2002, for more details).

The current data set including the HD140283 upper limit may be consistent with curve C, corresponding to strong shocks with hard CR spectra (expected in case the preshock gas is efficiently cooled by radiation), or a total SF CR energy a factor of ∼2.7 below the estimates described above

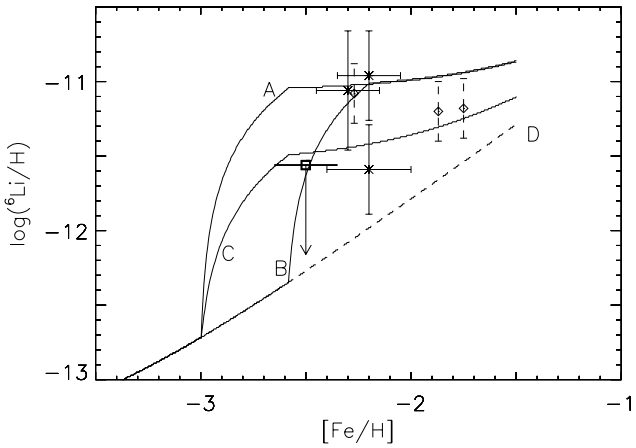

Fig. 4. Current observational data for ^{6}Li/H vs. [Fe/H] in Pop. II stars, compared with different models. The square, crosses and triangles correspond to the Subaru HDS upper limit for HD 140283, previous positive detections, and tentative VLT/UVES detections of Asplund et al. (2001), respectively. Model curves show the mean abundance predictions for SN CRs only (D, dashed), and SN plus SF CRs (A, B, C). Labels correspond to the following sets of parameters for $t_{\rm SF}$ [Gyr], $\tau_{\rm SF}$ [Gyr] and $\gamma_{\rm SF}$: A (0.22, 0.1, 3), B (0.32, 0.1, 3) and C (0.22, 0.1, 2).

(implying a lower total halo mass after the merger). If the steep rise of ^{6}Li is real, curve B may be a better representation, where the main SF shock at the final major merger occurs near [Fe/H] ∼ −2, possibly being compatible with some other lines of evidence (e.g. Chiba & Beers 2000). For conclusive tests of the SF shock picture, more detailed and less parameterized modelling utilizing e.g. numerical simulations of galaxy formation is necessary. A further crucial prediction of the scenario is correlations between the ^{6}Li abundance and the kinematic properties of Pop. II stars, which may also provide interesting insight into how the Galaxy formed.

The low upper limit for HD 140283 is an important addition to the observational database for ^{6}Li in Pop. II stars. However, it is still insufficient for discriminating between different production models, especially in view of the uncertain extent of depletion. To elucidate the true origin of ^{6}Li as well as the effects of stellar depletion in Pop. II stars, it is essential to obtain high quality data for a larger sample of stars with a wide range of metallicities and higher surface temperatures, an important goal for instruments such as the Subaru HDS.

5. Conclusions

We have obtained a high-S/N (900–1100), high-resolving-power (R = 95 000) spectrum of the metal-poor subgiant HD 140283 using HDS on the 8.2 m Subaru telescope, in an effort to measure its ^{6}Li/^{7}Li isotope ratio. We computed synthetic spectra using a 1-D model-atmosphere code, and used a χ^2 test to find the best fitting parameters. We find an isotope ratio consistent with zero, ^{6}Li/^{7}Li = 0.001, with an upper limit of ^{6}Li/^{7}Li < 0.018 estimated by a Monte Carlo analysis.

This measurement supersedes an earlier detection ($0.040 \pm 0.015(1\sigma)$) by one of the authors (Deliyannis & Ryan 2000). HD 140283 provides no support for the suggestion that Pop. II stars may preserve their ^{6}Li on the portion of the

subgiant branch where ^{7}Li is preserved. However, this star does not defeat the suggestion either; being at the cool end of subgiant branch of the Spite plateau, it may be sufficiently cool that ^{6}Li depletion has already set in, or the star may be sufficiently metal poor that little Galactic production of ^{6}Li had occurred. Continued investigation of other subgiants is necessary to test this idea.

We also consider the HD 140283 upper limit along with other measurements in the context of ^{6}Li production models, particularly the structure formation shock scenario, in which unique evolutionary trends can be expected without any direct relation to the abundances of Be, B, CNO or Fe. If HD 140283 has not been depleted in ^{6}Li, the upper limit can impose interesting constraints on the epoch and efficiency of dissipative dynamical processes that occurred during the formation of the Galaxy. Further observations together with improved theoretical modeling should allow us to test the structure formation scenario more critically and quantitatively, and to assess the value of ^{6}Li as a dynamical probe of the early Galaxy.

Acknowledgements. S.G.R. acknowledges numerous discussion with Dr C. P. Deliyannis on lithium processing in stars. This work was supported financially by PPARC (PPA/O/S/1998/00658) and the Nuffield Foundation (NUF-URB02). The high quality spectrum of HD 140283 used in the present study was obtained in a commissioning run of the HDS instrument group. S.I. acknowledges financial support from the Foundation for Promotion of Astronomy.

References

Asplund, M., Lambert, D. L., Nissen, P. E., Primas, F., & Smith, V. V. 2001, Cosmic Evolution, ed. E. Vangioni-Flam, R. Ferlet, & M. Lemoine (New Jersey: World Scientific), 95
Asplund, M., Nordlund, Å, Trampedach, R., & Stein, R. F. 1999, A&A, 346, L17
Boesgaard, A. M., Deliyannis, C. P., King, J. R., et al. 1999, AJ, 117, 1549
Bonifacio, P., & Caffau, E. 2003, A&A, 399, 1183
Cayrel, R., Spite, M., Spite, F., et al. 1999, A&A, 343, 923
Chiba, M., & Beers, T. C. 2000, AJ, 119, 2843
Cottrell, P. L., & Norris, J. 1978, ApJ, 221, 893
Deliyannis, C. P. 1990, Ph.D. Thesis, New Haven: Yale Univ.
Deliyannis, C. P., Boesgaard, A. M., Stephens, A., et al. 1998, ApJ, 498, L147
Deliyannis, C. P., & Malaney, R. A. 1995, ApJ, 453, 810
Deliyannis, C. P., & Ryan, S. G. 2000, BAAS, 196, 602
Duncan, D. K., Primas, F., Rebull, L. M., et al. 1997, ApJ, 488, 338
Fields, B. D., & Olive, K. A. 1999, ApJ, 516, 797
Fields, B. D., Olive, K. A., & Schramm, D. N. 1994, ApJ, 435, 185
Ford, A., Jeffries, R. D., Smalley, B., et al. 2002, A&A, 393, 617
Gray, D. F. 1992, The Observation and Analysis of Stellar Photospheres, 2nd edn (Cambridge: Cambridge University Press)
Hobbs, L. M., & Thorburn, J. A. 1994, ApJ, 428, L25
Hobbs, L. M., & Thorburn, J. A. 1997, ApJ, 491, 772
Hobbs, L. M., Thorburn, J. A., & Rebull, L. M. 1999, ApJ, 523, 797
Nissen, P. E., Asplund, M., Hill, V., & D'Odorico, S. 2000, A&A, 357, L49
Nissen, P. E., Lambert, D. L., Primas, F., & Smith, V. V. 1999, A&A, 348, 211
Noguchi, K., Aoki, W., Kawanomoto, S., et al. 2002, PASJ, 54, 855
Pilachowski, C. A., Sneden, C., & Booth, J. 1993, ApJ, 407, 699
Prantzos, N., Casse, M., & Vangioni-Flam, E. 1993, ApJ, 403, 630
Ramaty, R., Kozlovsky, B., & Lingenfelter, R. E. 1996, ApJ, 456, 525
Ramaty, R., Kozlovsky, B., Lingenfelter, R. E., & Reeves, H. 1997, ApJ, 488, 730
Ramaty, R., Lingenfelter, R. E., & Kozlovsky, B. 2000, The Light Elements and their Evolution, ed. L. da Silva, M. Spite, & J. R. de Medeiros (San Francisco: ASP), IAU Symp., 198, 51
Ramaty, R., Scully, S. T., Lingenfelter, R. E., & Kozlovsky, B. 2000, ApJ, 534, 747
Smith, V. V., Lambert, D. L., & Nissen, P. E. 1993, ApJ, 408, 262
Smith, V. V., Lambert, D. L., & Nissen, P. E. 1998, ApJ, 506, 405
Smith, V. V., Vargas-Ferro, O., Lambert, D. L., & Olgin, J. G. 2001, AJ, 121, 453
Steigman, G., & Walker, T. P. 1992, ApJ, 385, L13
Suzuki, T. K., & Inoue, S. 2002, ApJ, 573, 168
Suzuki, T. K., & Yoshii, Y. 2001, ApJ, 549, 303
Vangioni-Flam, E., Cassé, M., Cayrel, R., et al. 1999, New Astron., 4, 245
Vangioni-Flam, E., Lehoucq, R., & Cassé, M. 1994, The Light Element Abundances, ed. P. Crane (Berlin: Springer-Verlag), 389
Walker, T. P., Mathews, G. J., & Viola, V. E. 1985, ApJ, 299, 745
Yoshii, Y., Kajino, T., & Ryan, S. G. 1997, ApJ, 485, 605